Quantitative reconstruction of pore pressure history in sedimentary basins using fluid escape pipes

Joe Cartwright[1], Chris Kirkham[1], Martino Foschi[1], Neil Hodgson[2], Karyna Rodriguez[2] and David James[3]

[1] Department of Earth Sciences, University of Oxford, South Parks Road, Oxford, OX1 3 AN, UK

[2] Searcher, Unit 6, Albion House, High Street, Woking, GU21 6BG

[3] Cwmystwyth, Ceredigion, Wales

ABSTRACT

We present a novel method to reconstruct the pressure conditions responsible for the formation of fluid escape pipes in sedimentary basins. We analyse the episodic venting of high pressure fluids from the crests of a large anticlinal structure that formed off the coast of Lebanon in the past 1.7myrs. 21 fluid escape pipes formed at intervals of 50-100ka and transected over 3km of claystone and evaporite sealing units to reach the seabed. From fracture criteria obtained from nearby drilling we calculate that overpressures in excess of 30MPa were required for their formation, with pressure recharge of up to 2MPa occurring after each pipe forming event, resulting in a saw-tooth pressure-time evolution. This pressure-time evolution is most easily explained by tectonic overpressuring due to active folding of the main source aquifer whilst in a confined geometry.

INTRODUCTION

Fluid escape pipes (FEPs) are widely recognised in sedimentary basins as representing direct evidence for highly focused fluid venting to the surface from some deeper, overpressured source region (Loseth et al. 2011; Cartwright and Santamarina, 2015). To date, however, there has been no quantitative analysis of the pore pressure conditions leading to FEP formation.

Here we quantify the pore pressure conditions leading to the formation of a suite of FEPs from the Eastern Mediterranean (Fig. 1). These FEPs have previously been described by Cartwright et al. (2018) and Kirkham et al. (2019), but these studies did not provide any quantitative analysis of the deeper basinal pressure regime leading to their formation. Remarkably, these FEPs occur as a linear trail that represents the interplay between an episodic fluid venting process and a flowing salt layer, whereby each successively forming FEP is deformed and translated basinward by the flowing salt layer (Fig. 2). Their episodic occurrence is also unexplained since it has implications for the nature of the underlying causal pressure regime.

The observation that the FEPs transect a thick evaporite seal unit implies that they formed through propagation of hydraulic fracture networks in the sealing sequences (Kirkham et al. 2018). From this interpretation we are then able to derive a quantitative method to reconstruct the pore pressure history during their formation. This method only requires good first order description of FEP geometry and stratigraphic context, allied to calibration of material properties of the main rock units transected by any given FEP, and as such should be widely applicable to many other basinal contexts where similar FEPs occur. Quantifying the magnitude and evolution of pore pressure using the occurrence of FEPs as geological 'piezometers' adds a novel observational constraint to more conventional numerical modelling approaches to pore pressure evaluation in sedimentary basins.

GEOLOGIC SETTING

The study area is in the North Levant Basin (NLB) (Fig. 1), in the Eastern Mediterranean, where a c. 1.5km thick Messinian Evaporite sequence was deposited during the Messinian Salinity Crisis (MSC) (Gvirtzman et al. 2017). The immediate pre-salt stratigraphy consists of a c. 3km thick Oligo-Miocene clastic succession (Nader, 2011). Turbiditic sandstones of Late Oligocene to Early Miocene age form the reservoirs hosting ~35 Tcf of largely biogenic gas in a number of gas fields located 50-100km south of the study area (Fig. 1A), and are hydrostatically pressured

(Needham et al. 2017). These reservoirs are vertically sealed by Mid-Late Miocene claystones and Messinian Evaporites. The Pliocene to Recent succession is a largely fine-grained, prograding shelf-slope succession (Ghalayini et al. 2018).

The structure of the NLB is dominated by the thick detachment within the Messinian Evaporites (Fig. 1B). The pre-salt structure consists an array of NE-SW trending anticlines flanked by steeply dipping reverse faults, and NW-SE trending minor normal faults (Fig. S1)(Ghalayini et al. 2017). These folds formed during a late Neogene phase of basin wide compressional reactivation linked to activity on the Dead Sea Transform (Gardosh and Druckman, 2008; Gomez et al. 2007). Recognition of syn-kinematic reflection geometry within the Miocene together with significant fold amplitude at the Base Salt (Fig. 2A), implies a two-stage compressional history with a Late Miocene phase followed by a second phase of growth within the past 2-3 million years (Kirkham et al. 2019) coeval with regional folding (Hall et al., 2005; Gomez et al., 2007).

THE OCEANUS FEP TRAIL

A total of 21 FEPs that emanate from the structural crest of the pre-salt anticline (Fig. 2; Fig. S2), referred to as Oceanus (Fig. 1), have been identified in the NLB (Cartwright et al. 2018; Kirkham et al. 2019). The maximum relief of Oceanus is 660m, recorded at a Base Mid Miocene horizon, and that at the base salt is 320m, with a syn-kinematic mid-late Miocene sequence accounting for this difference in relief (Fig. 2).

The FEPs are seismically imaged in the post-salt overburden as cylindrical zones of disrupted reflectivity with a diameter of 100-300m (Fig. 2A) and are interpreted to have propagated across > 3km of Miocene claystones, Messinian Evaporites and Plio-

Pleistocene claystones (Fig. 2B). They are poorly imaged in the salt because they have been sheared by the flow of the salt, although the oldest (Pipe 1) is imaged as a high amplitude positive reflection, dipping shallowly through the salt (Fig. 2A).

The pockmark at the top of each FEP records the expulsion of fluids at the contemporaneous seabed, dating from 1.7Ma to the present day (Fig. 2). These pockmarks young progressively SE along the pipe trail (Fig. 2). Individual pockmarks cannot be dated precisely, but from measured pockmark spacing along the trail, and assuming a constant flow velocity (2mm/yr) of the salt (Kirkham et al. 2019) the venting episodes occurred at intervals of 50-100Ka (Fig. S2).

RECONSTRUCTION OF PORE PRESSURE EVOLUTION

It has previously been argued that because the FEPs transect the thick salt, and the fluid flow velocity at the surface outlet is sufficient to erode a crater at the seabed (pockmark), then the FEPs must have formed by hydraulic fracturing of all the units transected by individual FEPs (Kirkham et al., 2018; Cartwright et al. 2018)(see Data Repository). Hence we reconstructed the pressure conditions necessary for FEP formation assuming that pipe propagation required pressure conditions high enough to initiate and propagate hydraulic fracture networks across the stratigraphic interval transected by the Oceanus FEP trail. The Oceanus anticline is undrilled, and so to reconstruct the pressure conditions we used fracture gradient values (Oligo-Miocene - 23 MPa/km; Messinian Evaporites – 21 MPa/km) compiled and modelled for the nearby (50 km south; Fig. 1A) Tamar Gas Field (see Data Repository). Lateral seismic correlation indicates a high degree of similarity in the pre-salt stratigraphy of these two neighbouring areas of the basin. The source of the fluid and hence the position of the overpressured reservoir is assumed to be Lower Miocene sandstones, equivalent to the reservoirs calibrated and dated in the Tamar Gas Field (Needham et al., 2017).

The fluid pressure (Pf) in the top of the reservoir needed to form a FEP that propagates to surface is given by the standard criterion for hydraulic fracturing, which in a simplified form is expressed as Pf > σ_{min} + T, where σ_{min} is the minimum confining stress, and T is the tensile strength (Price and Cosgrove, 1990). In subsurface drilling, Pf can be calculated from the leak off pressure obtained during leak off tests and these values are compiled to define the fracture gradient for a given hydrocarbon field (Zhang and Yin, 2017). For the salt layer, we note that σ_{min} is likely to be within 1-3MPa of the overburden stress because salt is unable to sustain large differential stresses (Weijermars and Jackson, 2014), hence we used a value of overburden stress minus this window of 1-3 MPa for the fracture gradient within the salt, and assumed that T was effectively zero (Zhang and Yin, 2017).

Using a depth converted seismic profile, we computed depths to all the main formation boundaries as input to construct the pore pressure versus depth (P-z) plot (Gluyas and Swarbrick, 2004) for the present day structure at Oceanus, representing the conditions governing the formation of Pipe 21 (Fig. 3A). This plot shows that a minimum fluid pressure of 81.2 +/- 1MPa was required to initiate FEP propagation at the top of the Early Miocene reservoir (see Data Repository). Fluid pressures in excess of this value may have been necessary to achieve upward propagation of this pipe through the salt because the fracture gradient is close to the lithostatic gradient within the salt (Fig. 3A), but since we cannot calculate dynamic pressure gradients, we make a conservative assumption and take the value given by the intersection of the fracture gradient with the top reservoir (c.f. Watts, 1983).

To reconstruct the pressure conditions governing the formation of Pipe 1 (Fig. 3B), we applied the same approach, but took measured thicknesses and depths of the main stratigraphic units from a depth section across Oceanus restored to its geometry 1.7Ma ago (Fig. S3). We used the same fracture gradient values for the Miocene clastics and evaporites, but the depth values differed by removing 125m of post-salt overburden, and increasing salt thickness by 320m by restoring the Late Pliocene to Recent folding (Kirkham et al. 2019). The calculated pressure value for Pipe 1 is 85.3 +/- 1 MPa, some 4MPa higher than for Pipe 21 due to thicker salt in the 1.7Ma restoration (Fig. S3).

Finally, we used the pressure depth plots constructed for the start and end of the episodic FEP formation (Fig. 3) to reconstruct the evolution of fluid pressure from 1.7Ma to the present day, presented in the form of a pressure-time (P-t) plot (Fig. 4). This reconstructed P-t plot is based on the fixed conditions for the first and last FEP to form, and inferred pressure conditions for the 19 intervening FEPs that form at intervals of 50-100kyrs over the 1.7Ma time span of the FEP trail (Kirkham et al. 2019; Fig. S2). We assume a hydrostatic initial reservoir pressure (52 MPa) at the end of the MSC (at 5.33Ma)(Fig. 4A), based on measurement of hydrostatic reservoir pressures in nearby gas fields in reservoir units of similar age and burial history (Needham et al. 2017), implying a c. 30 MPa pressure increase was needed to form Pipe 1. Higher initial pressure is certainly possible, e.g. remnant overpressures resulting from the rapid loading/unloading events in the MSC (Bertoni et al., 2015), but this would reduce the additional pressure required not the total magnitude.

DISCUSSION

We reconstructed the P-t evolution in Figure 4 assuming that each FEP formed in response to a slower build-up and a rapid pressure release as fluids are expelled via the FEP (c.f. Kanno and Ichihara, 2018). This ‘saw-tooth’ pattern of episodic slow build and rapid release of pressure is characteristic of other natural phenomena involving venting of high pressure fluids from depth (Tait et al. 1989; Rocco et al. 2016).

We suggest two possible end members for this ‘saw-tooth’ pattern: (1) the pressure build-up between episodes is at a constant rate (Fig. 4B), or (2) the pressure drop after each venting episode is constant, and set here at an assumed 2MPa closure pressure to re-seal the reservoir as the hydraulic fractures close (Fig. 4C)(Hubbert and Willis, 1972). For (1), variable pressure drops might reflect heterogeneity in the FEP fracture network, and for (2), variable pressure build-up rates might result from irregularities in the boundary conditions leading to pressure recharge.

Of the various overpressure mechanisms that could be invoked to explain pipe formation (Osborne and Swarbrick, 1997), we considered four possible contributors: 1) disequilibrium compaction due to sediment loading; 2) hydrocarbon (gas) buoyancy; 3) marginal uplift leading to increased elevation head, and: 4) tectonic overpressuring due to a switch from vertical to horizontal maximum compressive stress. We argue against the first three mechanisms for the following reasons:

1) Disequilibrium compaction - could only have exerted a minimal influence (< 2MPa total) because of the modest thickness (355m) of post-salt sediments.
2) Hydrocarbon buoyancy - even if filled to spill, with a trap capacity of 340m (Fig. S3) at 1.7Ma the buoyancy pressure (3 MPa; Fig. 3B) would be too small. Buoyancy could however contribute to pressure recharge between each FEP forming event.

3) Marginal uplift - the reservoir is laterally confined and does not connect to uplifted older aquifers, making overpressuring by increasing elevation head unlikely (Walley, 1998; Nader, 2011).

Tectonic overpressuring requires active compression of a reservoir in a laterally confined and vertically sealed configuration such that the additional stress of horizontal compression is partly converted into pore fluid overpressure, with the magnitude of overpressure directly linked to the magnitude of horizontal stress (Mandl, 1988; Couzens-Schultz et al. 2014). Since the latest phase of folding of Oceanus correlates with the onset of the mid-Pliocene regional phase of folding (Gomez et al., 2007), and just precedes formation of the Pipe 1, it is therefore plausible that the switch to horizontal maximum compressive stress would have led to tectonic overpressuring of this confined reservoir. The magnitude of the increase possible with tectonic overpressuring is not known, but numerical modelling suggests that overpressures of 10-20MPa can be generated by < 10% of shortening (Obrador-Prats et al., 2017). In contrast to the other overpressure mechanisms we suggest that the necessary magnitude of 25-30 MPa of overpressure most likely occurred through tectonic overpressuring, although minor additional contributions from gas buoyancy and disequilibrium compaction cannot be excluded.

In summary, the documentation of the Oceanus pipe trail thus allows us to reconstruct the pressure history through time directly from geological observations, with only conservative assumptions, and further allows a quantitative evaluation of the mechanisms necessary to generate the requisite overpressures at depth. FEPs are observed in many sedimentary basins (Cartwright and Santamarina, 2015) and it seems likely that future observations of episodic fluid venting, particularly those connected to active tectonics should widen the potential for the analytical approach outlined in this study, and hopefully lead to a more holistic understanding of extreme overpressure development in the subsurface.

CONCLUSIONS

1. The palaeo-pressure conditions leading to episodic fluid venting from a highly overpressured source region can be reconstructed as pressure-depth (P-z) and pressure-time (P-t) plots using linear FEP trails in the Levant Basin.

2. The preferred mechanism to achieve the magnitude of overpressures involved to hydraulically fracture through 3 km of claystone and evaporites (1.5 km) from the Oceanus anticline is tectonic overpressuring during folding.

3. Episodic formation of FEPs is attributed to a saw-tooth pressure evolution with build-up and re-charge largely due to tectonic overpressuring with minor contributions possible from gas buoyancy and disequilibrium compaction.

ACKNOWLEDGMENTS

We are grateful to the editor Mark Quigley and the reviewers Sayed Behbehani, Peter Eichhubl and an anonymous reviewer for their constructive feedback that led to improvements in the paper. We acknowledge TGS for provision of the 3D seismic data. We thank Schlumberger for provision of the seismic interpretation software.

FIGURE CAPTIONS

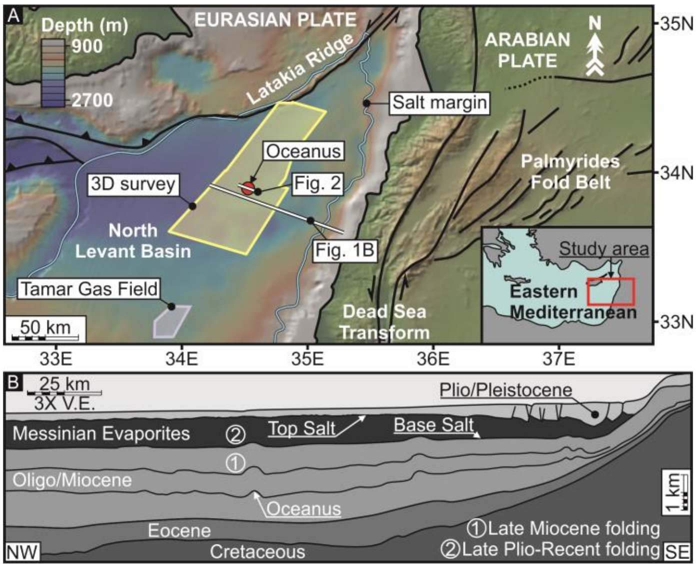

Figure 1: Geological setting of the study area. A: A bathymetric map (from GeoMapApp www.geomapapp.org), with the main structural elements. The location of a major pre-salt anticline (Oceanus) and the Tamar Gas Field are highlighted. B: A regional cross section showing the regional detachment within the thick Messinian Evaporites and the uplifted basin margin.

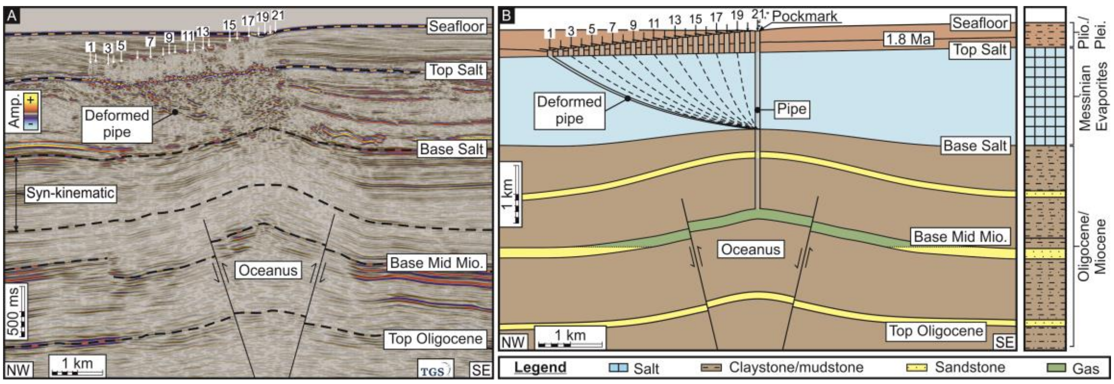

Figure 2: The Oceanus anticline and fluid escape pipe (FEP) trail. A: A seismic profile (location in Fig. 1A) through Oceanus and the FEP trail. Numbered white arrows point to pockmarks at the outlet of each FEP, numbered 1-21 in order of

formation. A syn-kinematic reflection geometry is present in the mid-late Miocene sequence. Pronounced relief at the Base Salt contrasts with the Top Salt geometry. B: Depth converted section through Oceanus and the FEP trail, with a simplified stratigraphic column. Dashed lines in the Messinian Evaporites represent deformed FEPs.

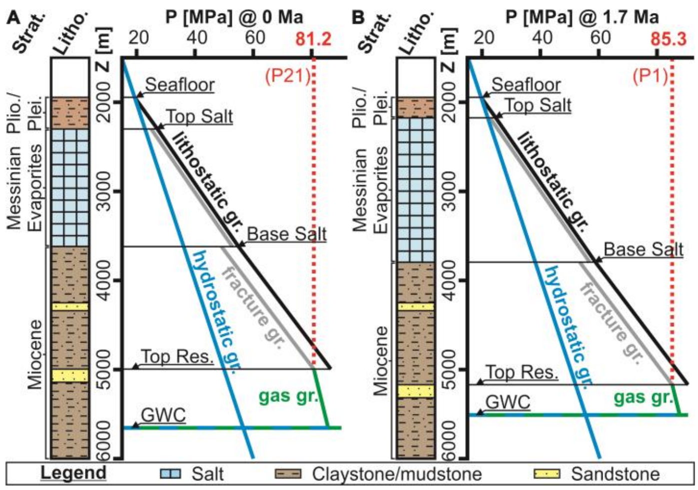

Figure 3: Pressure depth (P-z) plots for FEP formation above the Oceanus anticline. A: P-z plot for the last FEP (P21) in the trail, based on a reservoir filled with gas to its current trap capacity of 660m. 81.2 MPa is the pressure for FEP propagation across the topseal (intersection of the gas gradient with the fracture gradient). B: P-z plot for the first FEP (P1) to form, with a gas column of 340m equal to trap capacity reconstructed at 1.7Ma. GWC – Gas water contact; Res. – Reservoir; gr. – gradient.

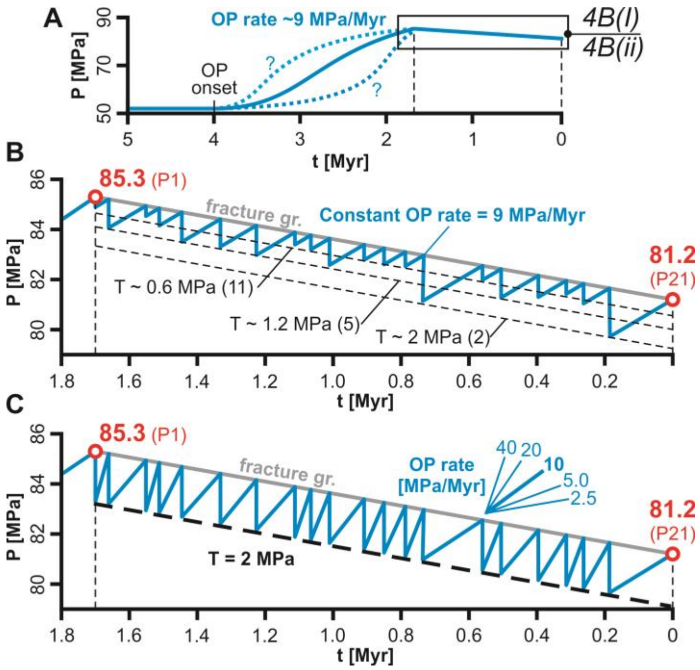

Figure 4: Pressure evolution for the Early Miocene reservoir at the crest of Oceanus. A: Gross pressure evolution from 5Ma to the present day, showing a possible pressure build-up curve (solid blue line) with hypothetical upper and lower bounds (dotted lines) from a starting point of hydrostatic pressure building to the overpressure value required for FEP formation. B&C: Reconstruction of the pressure evolution from 1.7Ma to illustrate two possible end member 'saw tooth' scenarios (see text). Upper bound defined by fracture gradient, OP rate is the pressure build-up rate in the reservoir. FEPs are dated based on an assumed constant salt flow velocity (Kirkham et al. 2019).

REFERENCES

Bertoni, C., and Cartwright, J., 2015, Messinian evaporites and fluid flow: Marine and Petroleum Geology, v. 66, p. 165-176, doi:10.1016/j.marpetgeo.2015.02.003.

Cartwright, J., Kirkham, C., Bertoni, C., Hodgson, N., and Rodriguez, K., 2018, Direct calibration of salt sheet kinematics during gravity-driven deformation: Geology, v. 46, p. 623-626, doi:10.1130/G40219.1.

Cartwright, J., and Santamarina, C., 2015, Seismic characteristics of fluid escape pipes in sedimentary basins: implications for pipe genesis: Marine and Petroleum Geology, v. 65, p. 126-140, doi:10.1016/j.marpetgeo.2015.03.023.

Couzens-Schultz, B. A., and Azbel, K., 2014, Predicting pore pressure in active fold–thrust systems: An empirical model for the deepwater Sabah foldbelt: Journal of Structural Geology, v. 69, p. 465-480, doi:10.1016/j.jsg.2014.07.013.

Gardosh, M. A., and Druckman, Y., 2006, Seismic stratigraphy, structure and tectonic evolution of the Levantine Basin, offshore Israel: Geological Society, London, Special Publications, v. 260, p. 201-227, doi:10.1144/GSL.SP.2006.260.01.09.

Ghalayini, R., Homberg, C., Daniel, J., and Nader, F., 2017, Growth of layer-bound normal faults under a regional anisotropic stress field: Geological Society, London, Special Publications, v. 439, p. 57-78, doi:10.1144/SP439.13.

Ghalayini, R., Nader, F., Bou Daher, S., Hawie, N., and Chbat, W., 2018, Petroleum systems of Lebanon: an update and review: Journal of Petroleum Geology, v. 41, p. 189-214, doi:10.1111/jpg.12700.

Gluyas, J. and Swarbrick, R. 2004. Petroleum Geoscience. Blackwells, Oxford.

Gomez, F., Nemer, T., Tabet, C., Khawlie, M., Meghraoui, M., and Barazangi, M., 2007, Strain partitioning of active transpression within the Lebanese restraining bend of the Dead Sea Fault (Lebanon and SW Syria): Geological Society, London, Special Publications, v. 290, p. 285-303, doi:10.1144/290.10.

Gvirtzman, Z., Manzi, V., Calvo, R., Gavrieli, I., Gennari, R., Lugli, S., Reghizzi, M., and Roveri, M., 2017, Intra-Messinian truncation surface in the Levant Basin explained by subaqueous dissolution: Geology, v. 45, p. 915-918, doi:10.1130/G39113.1.

Hall, J., Calon, T., Aksu, A., and Meade, S., 2005, Structural evolution of the Latakia Ridge and Cyprus Basin at the front of the Cyprus Arc, eastern Mediterranean Sea: Marine Geology, v. 221, p. 261-297, doi:10.1016/j.margeo.2005.03.007.

Hubbert, M. K., and Willis, D. G., 1972, Mechanics of hydraulic fracturing: AIME Petroleum Transactions, Society of Petroleum Engineers, v. 210, p. 153-168.

Kanno, Y., and Ichihara, M., 2018, Sawtooth wave-like pressure changes in a syrup eruption experiment: implications for periodic and nonperiodic volcanic oscillations: Bulletin of Volcanology, v. 80, p. 65, doi:10.1007/s00445-018-1227-z.

Kirkham, C., Cartwright, J., Bertoni, C., Rodriguez, K., and Hodgson, N., 2019, 3D kinematics of a thick salt layer during gravity-driven deformation: Marine and Petroleum Geology, v. 110, p. 434-449, doi:10.1016/j.marpetgeo.2019.07.036.

Kirkham, C., Cartwright, J., Hermanrud, C., and Jebsen, C., 2018, The genesis of mud volcano conduits through thick evaporite sequences: Basin Research, v. 30(2), p. 217-236, doi:10.1111/bre.12250.

Løseth, H., Wensaas, L., Arntsen, B., Hanken, N.M., Basire, C. and Graue, K., 2011, 1000 m long gas blow-out pipes: Marine and Petroleum Geology, v. 28(5), p.1047-1060, doi:10.1016/j.marpetgeo.2010.10.001

Mandl, G., 1988, Mechanics of tectonic faulting, Elsevier Amsterdam, 169-187 p.

Nader, F. H., 2011, The petroleum prospectivity of Lebanon: an overview: Journal of Petroleum Geology, v. 34, p. 135-156, doi:10.1016/j.marpetgeo.2009.12.013.

Needham, D. L., Pettingill, H. S., and Christensen, C. J., 2017, The Tamar Giant Gas Field: Opening the Subsalt Miocene Gas Play in the Levant Basin: AAPG Special Volumes, v. 113, p. 221-256, doi:10.1306/13572009M1133688.

Obradors-Prats, J., Rouainia, M., Aplin, A. C., and Crook, A. J., 2017, Assessing the implications of tectonic compaction on pore pressure using a coupled geomechanical approach: Marine and Petroleum Geology, v. 79, p. 31-43, doi:10.1016/j.marpetgeo.2016.10.017.

Osborne, M. J., and Swarbrick, R. E., 1997, Mechanisms for generating overpressure in sedimentary basins: a reevaluation: AAPG bulletin, v. 81, p. 1023-1041, doi:10.1306/522B49C9-1727-11D7-8645000102C1865D.

Price, N.J., and Cosgrove, J.W., 1990, Analysis of geological structures, Cambridge University Press.

Rocco, S., Woods, A.W., Harrington, J. and Norris, S. 2016. An experimental model of episodic gas release through fracture of fluid confined within a pressurized elastic reservoir. Geophysical Research Letters, 44, doi:10.1002/2016GL071546.

Tait, S., Jaupart, C. and Vergniolle, S. 1989. Pressure, gas content and eruption periodicity of a shallow, crystallising magma chamber. Earth and Planetary Science Letters, 92, 107-123.

Walley, C. D., 1998, Some outstanding issues in the geology of Lebanon and their importance in the tectonic evolution of the Levantine region: Tectonophysics, v. 298, p. 37-62, doi:10.1016/S0040-1951(98)00177-2.

Watts, N. L., 1987, Theoretical aspects of cap-rock and fault seals for single- and two-phase hydrocarbon columns: Marine and Petroleum Geology, v. 4, p. 274-307, doi:10.1016/0264-8172(87)90008-0.

Weijermars, R., and Jackson, M. P., 2014, Predicting the depth of viscous stress peaks in moving salt sheets: Conceptual framework and implications for drilling: AAPG bulletin, v. 98, p. 911-945, doi:10.1306/09121313044.

Zhang, J., and Yin, S. X., 2017, Fracture gradient prediction: an overview and an improved method: Petroleum Science, v. 14, p. 720-730, doi:0.1007/s12182-017-0182-1.

Supplementary material for 'Quantitative reconstruction of pore pressure history in sedimentary basins using fluid escape pipes'

Joe Cartwright[1], Chris Kirkham[1], Martino Foschi[1], Neil Hodgson[2], Karyna Rodriguez[2] and David James[3]

[1] Department of Earth Sciences, University of Oxford, South Parks Road, Oxford, OX1 3 AN, UK

[2] Searcher, Unit 6, Albion House, High Street, Woking, GU21 6BG

[3] Cwmystwyth, Ceredigion, Wales

SEISMIC AND WELL DATA

A 3D seismic survey acquired and processed by Spectrum (now TGS) was used for the study, along with selected profiles from two regional 2D seismic surveys. The data was interpreted and all key horizons were mapped using Petrel software. Further details can be found in Cartwright et al. (2018) and Kirkham et al. (2019).

TIMING OF FOLD PHASES

The growth history of the Oceanus pre-salt anticline involves two main phases of tectonic compression linked to regional plate boundary changes. The first is evidenced by the syn-kinematic packages of the Mid to Late Miocene units thinning onto the fold crests. The second phase occurred during the Pliocene to Recent, and is evidenced by the substantial structural relief at the base of the salt sheet (Fig. 2; Fig. S3). Regional tectonic reconstructions of the Dead Sea Transform have suggested a renewed phase of activity from 3 Ma in the adjacent regions of Lebanon (Gomez et al. 2007), and the Latakia Ridge (Hall et al. 2005) which points to rejuvenated growth of offshore pre-salt anticlines occurring at approximately the same time. Continued growth of these folds during the critical period of the last 2 million years is thus consistent with the regional tectonic context, and would require a state of stress to be characterised by a horizontal and NW-SE oriented maximum compressive stress.

FORMATION OF FLUID ESCAPE PIPES BY NATURAL HYDRAULIC FRACTURING

A number of mechanisms have been suggested to explain the formation of fluid escape pipes, including hydraulic fracturing, solution collapse, and fluidisation (see review in Cartwright and Santamarina, 2015). For fluid escape pipes that transect thick salt sequences however, it has recently been argued that hydraulic fracturing offers the only plausible mechanism (Kirkham et al. 2018). This argument is based on the co-occurrence of fluid escape pipes with pockmarks and small mounded extrusive bodies (mud volcanoes) at their outlets in a region of the West Nile Delta, and where both sets of conduits transected a thick salt sequence en route from the source region to the contemporaneous seabed. Fluidisation is not viable in an evaporite layer, and solution collapse would only occur locally before brine saturations exceed the halite solubility threshold. Hydraulic fracture networks offer the only viable explanation for the fluxes implied by the extrusion of the mud volcanoes.

The fluid escape pipes in the study area are identical in their dimensions and seismic character to those described by Kirkham et al. (2018), and by analogy therefore, we assume that a similar formation mechanism applied. The detailed geometry of the postulated hydraulic fracture networks are unknown, however, so we simply assume that fluid pressures must have been sufficient to initiate and propagate small scale (10s of metres) hydraulic fractures in the generalised zone imaged by the seismic pipe structure (see Cartwright and Santamarina, 2015). This assumption underpins our use of the local fracture gradient in the sealing intervals above the reservoir to compute the minimum pressure required for pipe formation. This conservative view does not take into account possible complicating factors relating to multiphase flow, gas exsolution, or wall rock collapse. Similarly, we are not able to compute the dynamic pressure gradient of the fluid flowing upwards in the pipe.

METHODOLOGY FOR CONSTRUCTING THE PRESSURE-DEPTH AND PRESSURE-TIME PLOTS

The pressure-depth and pressure-time plots presented in Figures 3 and 4 were constructed for Oceanus with the following methodology. A seismic profile was extracted from the 3D seismic volume as an arbitrary line directed along the pipe trail. Key marker horizons on this profile were obtained from the results of previous studies (Cartwright et al. 2018; Kirkham et al. 2019) and were depth converted using interval velocities of 2000 m/s, 4,200 m/s, and 3000 m/s for the post-salt overburden (Pliocene to Recent), the salt layer (Messinian), and the pre-salt succession (Oligo-Miocene), respectively (Fig. 1B). These velocities were derived from data from nearby exploration wells (Kirkham et al. 2019).

Calculations of the hydrostatic and lithostatic pressure distribution with depth were based on a seawater density value of 1.06 g/cc, and 2.0, 2.15 and 2.35 g/cc for the post-salt, salt and pre-salt layers. The sediment densities were obtained from petrophysical measurements made on nearby wells in the Tamar Field (see Fig. 1A for location)(Needham et al. 2017). The fracture gradient for the Oligo-Miocene sealing interval was taken from modelled values for the Tamar Field (Needham et al. 2017, their Fig. 19). This is the nearest borehole calibration of the Oligo-Miocene succession in the North Levant Basin. Although the fracture gradient is not an actual value, we note that it exceeds the mudweights used in the wells, and is based on actual drilling experience in multiple exploration and appraisal wells. The fracture gradient for the salt layer is taken as 2MPa below the lithostatic value. No actual measurements were available for the salt in the North Levant Basin (e.g. from leak-off tests or mini-fracture tests- see Needham et al. 2017). However, compilations of these test data from drilling across a variety of thick salt layers shows that the fracture gradient is close to the lithostatic gradient, or in some cases exceeds that value (Zhang and Yin, 2017). Our assumption of a fracture gradient set at 2 MPa below lithostatic is thus conservative, and accords with estimates of the upper limit of differential stress within salt layers of 1-3 MPa (Weijermaars and Jackson, 2014; Schoenherr et al., 2007).

The depth converted section along the Oceanus pipe trail was restored to its geometry at 1.7Ma (the time of formation of the first pipe in the trail) by removing sediments younger than this age from the post-salt overburden, but maintaining a constant water depth. The actual water depth is not known, but by keeping water depth constant, this simply requires a small amount of subsidence during the past 1.7Ma, which is consistent with stratigraphic analysis of depositional environments in this period (Gardosh and Druckman, 2006) and regional geological modelling (Al Balushi et al. 2016). In addition to this backstripping of post 1.7Ma sediments, the section was restored by retro-deforming Oceanus anticline such that the structural relief at the base salt diminished to zero. This equates to removing the mid-Pliocene to Recent phase of fold amplification (Kirkham et al. 2019) but does not involve any movement of the top salt surface, which remains horizontal throughout. Hence the restored profile (Fig. S3A) shows a thicker salt succession above the underlying anticlinal axis than the present day section. The pressure-depth plot for this restored section (Fig. 3B) was constructed using the same input density values for the pre-salt, salt and post-salt layers as for the present day section. The fracture gradient within the Oligo-Miocene was adjusted to maintain a similar value (as a percentage of the lithostatic gradient) as in the pressure depth plot constructed based on the present day structural configuration (Fig. 3A).

The trap capacity of the Oceanus Structure at the present day was calculated (660m) by measuring the relief in metres from the spill point of the structure to the crest of the anticline as mapped at the reservoir level (Fig. S2). The trap capacity existing prior to the latest phase of fold amplification (340m) was obtained by subtracting the amplitude of the later phase of growth (equivalent to the structural relief at the base salt, 320m) from the present day trap capacity). Using these figures, indicative gas gradients were added to the two pressure-depth plots to show the minimal impact that a filled-to-spill gas column would have exerted on the top seal in comparison to the much larger aquifer overpressure (Fig. 3). The gas gradients were computed from measured gas pressures in appraisal wells on the Tamar Gas Field, where the reservoir is at a similar depth, and most likely similar pressure-temperature conditions as Oceanus (Needham et al. 2017).

The pressure-time plot was constructed by taking the two pressure-depth plots, and noting the intersection value of the fracture gradient with the depths to the top reservoir, and base salt for each plot. The critical pressure value was taken as the value at the top reservoir. These yielded 85.3 and 81.2 MPa, for the first and last pipe to form, respectively. Error bars on these values are estimated at +/- 3 MPa, but would be systematic for both time steps since they are based on error bars for seismic correlation and depth conversion.

The pressure evolution in the last 1.7Ma was constructed by taking the dates of the individual fluids escape pipes (see below), and interpolating two contrasting sawtooth patterns (see main text)(Kanno and Ichihara, 2018) between the starting and end point. In the first (Fig. 4B), the geometry of the ‘teeth’ is controlled by choosing a fixed pressure re-charge rate that matches rate during the build-up in overpressure leading to the first pipe forming event. The second (Fig. 4C) is defined by considering that the pressure drop for each ‘tooth’ is fixed and is equivalent to the fracture closure pressure or effective tensile strength (Hubbert, 1953). The effective tensile strength of the probable sealing claystones of the Oligo-Miocene are not known, but we set this to be 2 MPa, simply to illustrate one of many possible pressure evolutionary paths linking the two computed values.

SALT FLOW KINEMATICS

For Oceanus, the average flow velocity for the upper boundary of the salt layer was calculated from the biostratigraphic date for the horizon incised by the earliest pockmark, and the horizontal distance between the earliest and latest pockmark craters (3.4 km). These values give an average flow velocity of 2 (+/- 0.3) mm/a over the past 1.7 myrs (Cartwright et al. 2018). Pipe spacing was divided by average velocity for each individual trail to yield the timings of each pipe within each trail. These values were used to construct the pressure-time plot for Oceanus shown in Figure 4.

SUPPLEMENTARY FIGURES AND CAPTIONS

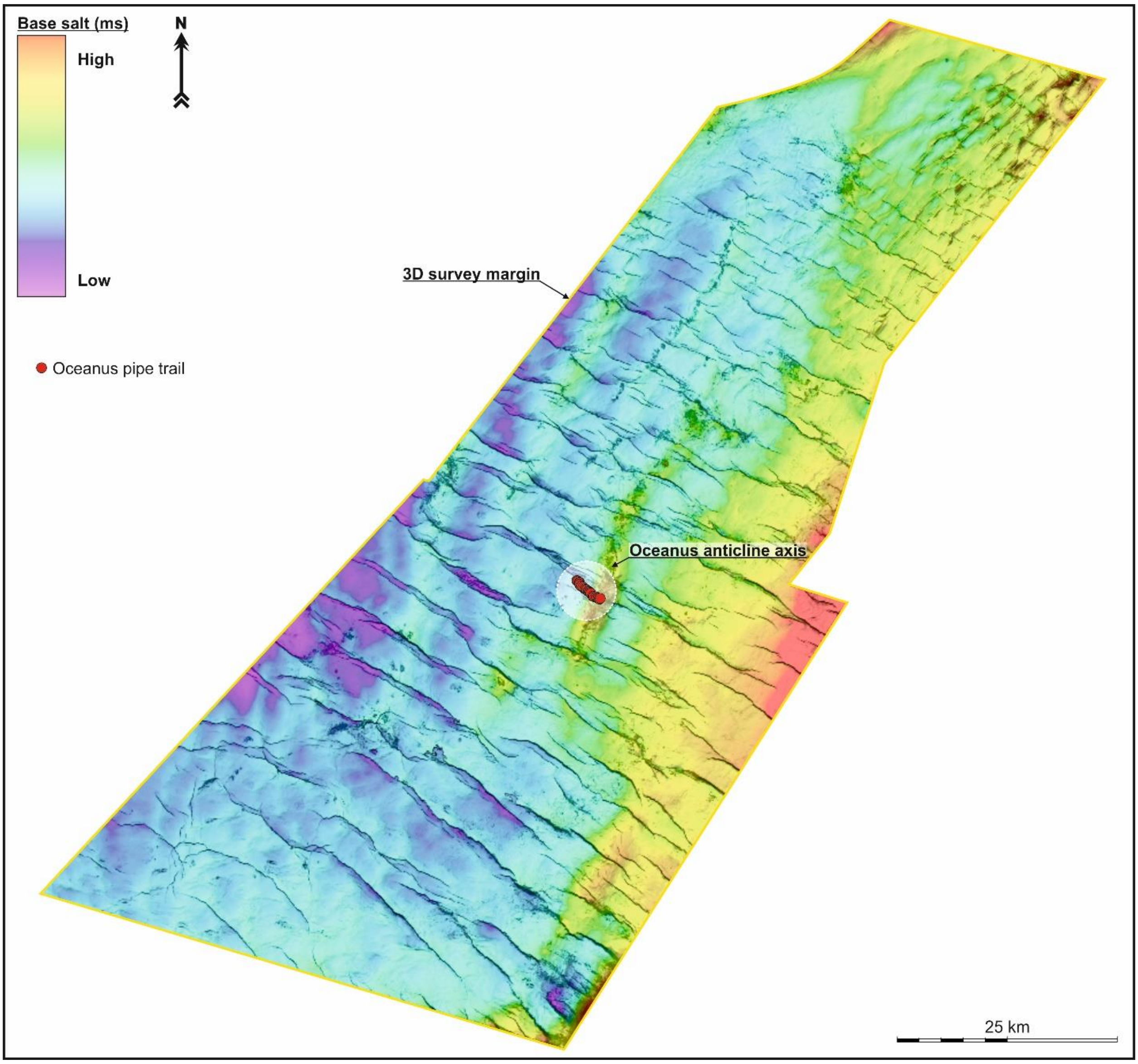

Figure S1: Two-way time Base Salt structure map (in milliseconds, ms) of the 3D survey in the study area, showing the location of the pre-salt anticline named Oceanus and the 21 fluid escape pipes that overly it. Also prominently visible are the WNW-ESE trending normal faults that are widely developed in the North Levant Basin.

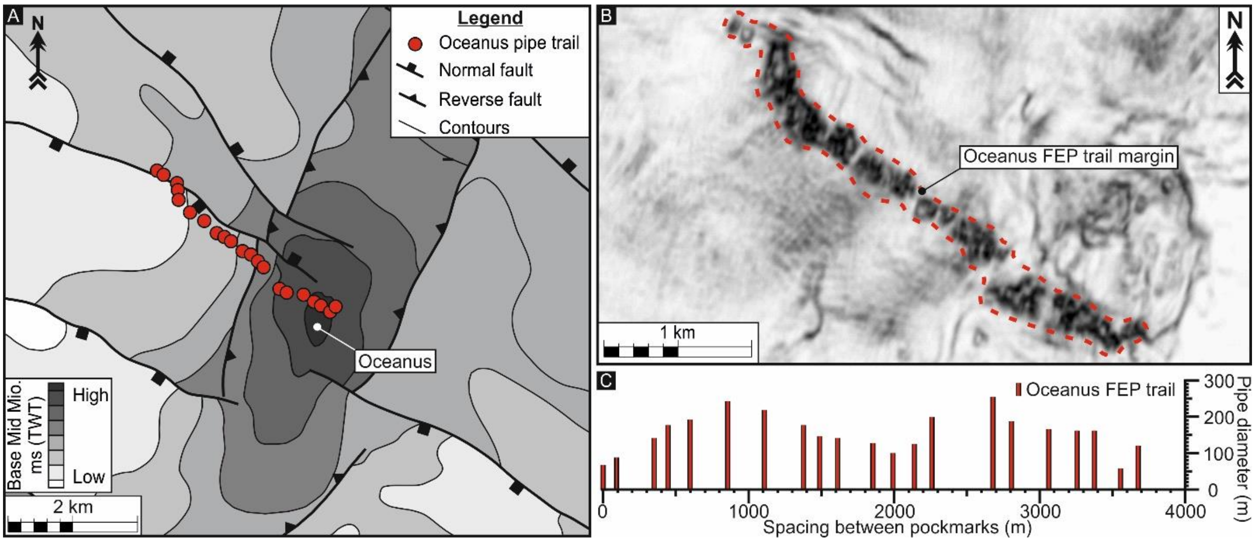

Figure S2: Detailed positions and spacing of the pockmarks associated with the fluid escape pipes trail overlying Oceanus. A: Structure map in two-way time (ms) of the Base Middle Miocene horizon (Modified from Cartwright et al. 2018) centred on Oceanus, showing the WNW orientation of the fluid escape pipe trail emanating from the crest of the anticline. The structure is aligned NNE-SSW, and bounded by reverse faults, and compartmentalised by WNW trending normal faults. B: A variance slice through the Pliocene to Recent overlying Oceanus, showing the WNW-ESE linear area of discontinuity attributed to the fluid escape pipe trail. C: Pockmark spacing data for the fluid escape pipe trail overlying Oceanus documented by Kirkham et al. (2019). These data were used to compute the ages of each pipe, for reconstruction of the pressure evolution over the past 1.7Myrs.

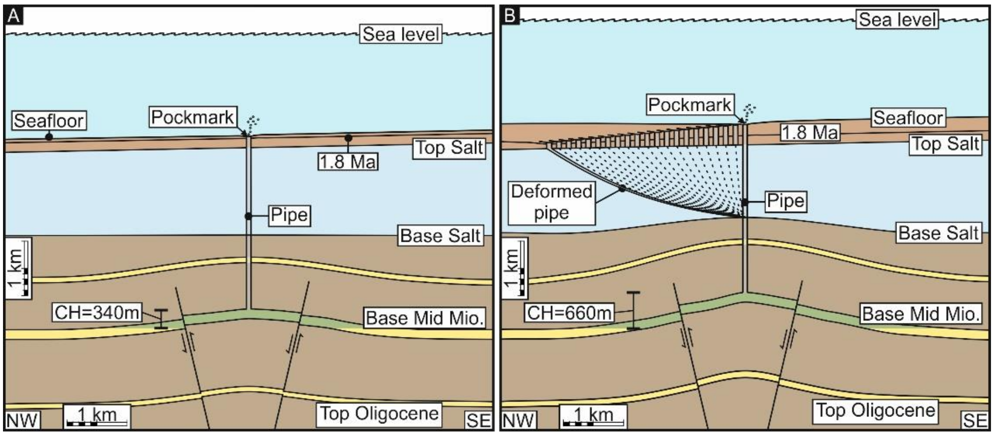

Fig. S3. Schematics of Oceanus and the fluid escape pipes at the first expulsion episode and most recent expulsion episode. A: A schematic restored depth cross-section of Oceanus at the timing (1.7 Ma) of initial pipe formation, with a trap capacity (CH=Column Height) of 340m. B: A schematic present day depth cross-section through Oceanus. Since initial pipe formation the top seal has episodically failed a further 20 time. Growth of the fold during the Pliocene to Recent has produced an increase in trap capacity to 660m, substantial structural relief at Base Salt and thinning of the overlying salt succession.

REFERENCES

Al-Balushi, A. N., Neumaier, M., Fraser, A. J., and Jackson, C. A., 2016, The impact of the Messinian salinity crisis on the petroleum system of the Eastern Mediterranean: a critical assessment using 2D petroleum system modelling: Petroleum Geoscience, v. 22, p. 357-379, doi:10.1144/petgeo2016-054.

Cartwright, J., Kirkham, C., Bertoni, C., Hodgson, N., and Rodriguez, K., 2018, Direct calibration of salt sheet kinematics during gravity-driven deformation: Geology, v. 46, p. 623-626, doi:10.1130/G40219.1.

Cartwright, J., and Santamarina, C., 2015, Seismic characteristics of fluid escape pipes in sedimentary basins: implications for pipe genesis: Marine and Petroleum Geology, v. 65, p. 126-140, doi:10.1016/j.marpetgeo.2015.03.023.

Gardosh, M. A., and Druckman, Y., 2006, Seismic stratigraphy, structure and tectonic evolution of the Levantine Basin, offshore Israel: Geological Society, London, Special Publications, v. 260, p. 201-227, doi:10.1144/GSL.SP.2006.260.01.09.

Ghalayini, R., Nader, F., Bou Daher, S., Hawie, N., and Chbat, W., 2018, Petroleum systems of Lebanon: an update and review: Journal of Petroleum Geology, v. 41, p. 189-214, doi:10.1111/jpg.12700.

Gomez, F., Nemer, T., Tabet, C., Khawlie, M., Meghraoui, M., and Barazangi, M., 2007, Strain partitioning of active transpression within the Lebanese restraining bend of the Dead Sea Fault (Lebanon and SW Syria): Geological Society, London, Special Publications, v. 290, p. 285-303, doi:10.1144/290.10.

Hall, J., Calon, T., Aksu, A., and Meade, S., 2005, Structural evolution of the Latakia Ridge and Cyprus Basin at the front of the Cyprus Arc, eastern Mediterranean Sea: Marine Geology, v. 221, p. 261-297, doi:10.1016/j.margeo.2005.03.007.

Hubbert, M. K., and Willis, D. G., 1972, Mechanics of hydraulic fracturing: AIME Petroleum Transactions, Society of Petroleum Engineers, v. 210, p. 153-168.

Kanno, Y., and Ichihara, M., 2018, Sawtooth wave-like pressure changes in a syrup eruption experiment: implications for periodic and nonperiodic volcanic oscillations: Bulletin of Volcanology, v. 80, p. 65, doi:10.1007/s00445-018-1227-z.

Kirkham, C., Cartwright, J., Bertoni, C., Rodriguez, K., and Hodgson, N., 2019, 3D kinematics of a thick salt layer during gravity-driven deformation: Marine and Petroleum Geology, v. 110, p. 434-449, doi:10.1016/j.marpetgeo.2019.07.036.

Kirkham, C., Cartwright, J., Hermanrud, C., and Jebsen, C., 2018, The genesis of mud volcano conduits through thick evaporite sequences: Basin Research, v. 30(2), p. 217-236, doi:10.1111/bre.12250.

Needham, D. L., Pettingill, H. S., and Christensen, C. J., 2017, The Tamar Giant Gas Field: Opening the Subsalt Miocene Gas Play in the Levant Basin: AAPG Special Volumes, v. 113, p. 221-256, doi:10.1306/13572009M1133688.

Schoenherr, J., Urai, J. L., Kukla, P. A., Littke, R., Schleder, Z., Larroque, J.-M., Newall, M. J., Al-Abry, N., Al-Siyabi, H. A., and Rawahi, Z., 2007, Limits to the sealing capacity of rock salt: A case study of the infra-Cambrian Ara Salt from the South Oman salt basin: AAPG bulletin, v. 91, p. 1541-1557, doi:10.1306/06200706122.

Weijermars, R., and Jackson, M. P., 2014, Predicting the depth of viscous stress peaks in moving salt sheets: Conceptual framework and implications for drilling: AAPG bulletin, v. 98, p. 911-945, doi:10.1306/09121313044.

Zhang, J., and Yin, S. X., 2017, Fracture gradient prediction: an overview and an improved method: Petroleum Science, v. 14, p. 720-730, doi:0.1007/s12182-017-0182-1.